STRUCTURAL CONTROL AND HEALTH MONITORING
Struct. Control Health Monit. 2016; **00**:1–24
Published online in Wiley InterScience (www.interscience.wiley.com). DOI: 10.1002/stc

Seismic FDD modal identification and monitoring of building properties from real strong-motion structural response signals

Fabio PIOLDI[1], Rosalba FERRARI[1], Egidio RIZZI[1,*]

[1] *Università degli Studi di Bergamo, Dipartimento di Ingegneria e Scienze Applicate (Dalmine), viale G. Marconi 5, I-24044 Dalmine (BG), Italy*

SUMMARY

In the present study, output-only modal dynamic identification and monitoring of building properties is attempted successfully by processing *REAL* earthquake-induced structural response signals. This is achieved through an enhanced version of a recently-developed *refined Frequency Domain Decomposition (rFDD)* approach, which in the earlier implementation was adopted to analyse *SYNTHETIC* seismic response signals only. Despite that *SHORT*-duration, *NON-STATIONARY* seismic response data and *HEAVY* structural damping shall not fulfil traditional Operational Modal Analysis (OMA) assumptions, the present rFDD response-only algorithm allows for the effective estimation of strong-motion natural frequencies, mode shapes and modal damping ratios, with real seismic response signals. The present rFDD enhancement derives from a pre-processing time-frequency analysis and from an integrated approach for PSD matrix computation, which constitute crucial innovative issues for the treatment of real earthquake response data. A monitoring case study is analysed by taking the real strong-motion response records from a 7-storey reinforced concrete building in Van Nuys, California, from 1987 to the latest 2014 events (CESMD database), as recorded before, during and after the 1994 Northridge earthquake, which severely damaged the building (then retrofitted). This paper proves the effectiveness of the proposed enhanced rFDD algorithm as a robust method for monitoring current structural modal properties under real earthquake excitations. This shall allow for identifying possible variations of structural features along experienced seismic histories, providing then a fundamental tool towards Earthquake Engineering and Structural Health Monitoring purposes.

Submitted: 11 April 2016; Revised: 09 September 2016 - Resubmitted: 21 November 2016

KEY WORDS: Operational Modal Analysis (OMA); refined Frequency Domain Decomposition (rFDD); Real earthquake response input; Strong-motion modal parameter identification; Estimated modal damping ratio.

1. INTRODUCTION

In the field of Earthquake Engineering and Structural Health Monitoring, the evaluation of current structural dynamic properties plays a fundamental role, especially for potential structural changes that strong-motion events and dynamic loadings may induce in civil infrastructures. These variations may be detected by prompt modal parameter estimates, through specific identification techniques that may deal not only with the pre- and post-earthquake stages, but also during sequences of ground

*Correspondence to: Egidio RIZZI, University of Bergamo, Department of Engineering and Applied Sciences (Dalmine), viale G. Marconi 5, I-24044 Dalmine (BG), Italy. Tel: +39.035.205.2325, Fax: +39.035.205.2310, email: egidio.rizzi@unibg.it

motion events. This aim is targeted in the present work, where the effectiveness of a dedicated response-only approach in the Frequency Domain is proven by processing real earthquake structural response signals.

The identification of structural dynamic properties at seismic input pursues various goals, as response prediction, condition assessment, Structural Control and Health Monitoring or damage identification [14–16, 18, 30, 39, 41, 47, 48, 53, 56]. Nearly all of the available attempts towards these ends pertain to the realm of Experimental Modal Analysis (EMA) [3, 4, 10, 17, 21, 27, 28], since they need the knowledge or measurement of the input ground motion. However, in most practical cases the true foundation input motion turns out to be unavailable or unreliable (e.g. not recorded, recorded with low signal-to-noise ratio or affected by Soil-Structure Interaction effects [63]).

In the field of Operational Modal Analysis (OMA), some researchers have investigated the use of strong ground motions in the Time Domain, as for instance [19, 20, 25, 35, 36, 40, 50, 54, 55, 60]. Rather, the output-only analysis in the Frequency Domain looks quite shortfall in the earthquake engineering range, especially as concerning to non-parametric algorithms (as FDD is). Few notable exceptions come from [34, 38, 39, 61]. Then, a few attempts performed OMA with general non-stationary signals, as for instance [2, 22, 23, 31].

The present paper deals with a *refined Frequency Domain Decomposition (rFDD)* technique, a considerable evolution of classical FDD algorithms [8, 9]. This work considers the effective processing of *REAL* (earthquake-induced) structural response signals, whereas previous underlying contribution [43], outlining the main body of the adopted methodology, was dealing with *SYNTHETIC* response signals only. The final adoption of real signals clearly opens up a new world here, and actually constitutes a typical final task within the validation of the proposed OMA identification procedure. The paper starts from the previous analysis with synthetic response signals and, after introducing novel dedicated strategies required for the handling of real seismic response signals (such as a pre-processing time-frequency analysis and an integrated approach for PSD matrix computation), arrives at demonstrating that modal identification becomes feasible in this field, by outlining SHM application scenarios based on the comprehensive analysis of a realistic monitoring case study considering pre-, during- and post-damaging earthquake structural conditions. In other words, this contribution closes the circle on the present research investigation devoted to the rather challenging framework of OMA modal identification based on earthquake-induced *SHORT*-duration, *NON-STATIONARY*, *HEAVY-DAMPED* structural response signals.

With respect to other common OMA techniques, FDD formulations have been quite widespread, due to simple implementation, computational set-up and user-friendliness [51]. Classical FDD procedures are centred on a Singular Value Decomposition (SVD) of the output Power Spectral Density (PSD) matrix [8], hence they pertain to non-parametric response-only methods [9, 64].

As well as most of existing OMA methods, classical FDD techniques are based on the hypothesis of long-duration stationary white noise input [5, 8]. Other typical assumptions are constituted by low structural damping (modal damping ratios $\zeta_i \ll 1$) and geometrically-orthogonal mode shapes of close modes [7, 8, 51]. Hence, in principle, classical FDD formulations should not be employed with short-duration and non-stationary input data, like those coming from earthquake responses, and also at simultaneous heavy damping, in the sense of identification challenge [8, 22].

Nevertheless, the present enhanced rFDD algorithm reduces typical disadvantages pertaining to traditional FDD formulations, by allowing for the consistent analysis with real earthquake-induced response signals and heavy damping within the OMA field. Thus, the application of this comprehensive rFDD approach looks appealing towards potential seismic monitoring purposes, within the challenging research scenario of Earthquake Engineering and Structural Health Monitoring.

In the paper, after a first validation step, still with simulated data, even considering Soil-Structure Interaction (SSI) effects, the monitoring analysis makes reference to real signals taken from the Center of Engineering Strong Motion Data (CESMD) database [11]. Specifically, the well-documented 7-storey RC building in Van Nuys, California, has been analysed. Several information and surveys on this structure may be found in [29, 32, 57–59]. Nine different earthquakes occurred from 1987 to 2014 have been considered here. The structural response signals coming from these

DOI: 10.1002/stc

excitations were split into two sets, "pre-retrofit" and "post-retrofit", since the 1994 Northridge earthquake did severely damage the building, which was afterwards retrofitted. The aim here is that to prove the efficiency of the present rFDD algorithm in dealing with real earthquake-induced response signals and to detect and monitor the time variation of the modal properties.

Presentation of the paper is structured as follows. Forthcoming Section 2 deals with main theoretical aspects of the present rFDD algorithm, with specific reference to the new pre-processing time-frequency analysis and to the novel integrated PSD matrix computation approach, which have been specifically developed to deal with real earthquake responses. Section 3 presents a first validation of the algorithm with simulated data from a 5-storey frame, considering also Soil-Structure Interaction effects. Section 4 outlines the real monitoring case-study under target and the adopted earthquakes shaking the structure, jointly with some remarks on the use and processing of real seismic-response signals. Section 5 derives comprehensive results on the application of the present rFDD approach to the selected real earthquake-induced response signals, considering outcomes from pre- and post-retrofit stages, in terms of monitoring purposes. In the end, main conclusions are gathered in Section 6.

2. FUNDAMENTALS OF THE rFDD ALGORITHM WITH REFERENCE TO REAL SEISMIC RESPONSE SIGNALS

Classical FDD validity hypotheses refer to white noise input, low modal damping ratios (ζ_i in the order of 1%) and geometrically-orthogonal mode shapes of "*close modes*"; see discussion in [8, 64].

The present rFDD approach addresses such use limitations, through original arrangements and strategies devised to tackle real seismic responses, at simultaneous heavy damping. The term "*heavy damping*" refers here to cases that set realistic structural damping, e.g. ζ_i in the order of 5%, but leading to rather challenging identification in the OMA Frequency-Domain framework (where typically only damping ratios in the order of $1\% - 2\%$ have been considered). In the following paragraphs, the crucial steps of the present rFDD technique are exposed, by rereading and reinterpreting its main formulation [42, 43]. The novel issues concerning the pre-processing time-frequency analysis and the integrated PSD matrix computation approach are presented, as enhancement of the method, towards achieving a more comprehensive framework and allowing for the treatment of real seismic response signals.

A first theoretical demonstration of the rFDD efficacy has been reported in [43]. In [44] the instantaneous Auto-Correlation Functions of the seismic records have been involved, too. Both studies referred only to synthetic earthquake response signals, in view of a necessary validation condition for the identification technique. In the present work, chief attention is focused on the novel pre-processing time-frequency analysis (see Section 2.1) and on the innovative integrated PSD computation (see Section 2.2), which are challenging and fundamental phases when dealing with real earthquake response signals.

2.1. *Time-Frequency signal analysis and refined FDD technique for real earthquake-induced response signals*

FDD algorithms basically rely on the general input/output spectral MDOF relationship [5]:

$$\mathbf{G}_{yy}(\omega) = \overline{\mathbf{H}}(\omega)\mathbf{G}_{xx}(\omega)\mathbf{H}^{\mathrm{T}}(\omega) \tag{1}$$

where $\mathbf{G}_{xx}(\omega)$ and $\mathbf{G}_{yy}(\omega)$ are the input and output PSD matrices, $\mathbf{H}(\omega)$ is the Frequency Response Function (FRF) matrix, while overbar and apex T denote complex conjugate and transpose, respectively. By adopting the pole/residue form of the FRF $\mathbf{H}(\omega)$ [5], Eq. (1) can be rewritten as:

$$\mathbf{G}_{yy}(\omega) = \left(\sum_{k=1}^{n} \frac{\overline{\mathbf{R}}_k}{-\mathrm{i}\,\omega - \overline{\lambda}_k} + \frac{\mathbf{R}_k}{-\mathrm{i}\,\omega - \lambda_k} \right) \mathbf{G}_{xx}(\omega) \left(\sum_{s=1}^{n} \frac{\mathbf{R}_s^{\mathrm{T}}}{\mathrm{i}\,\omega - \lambda_s} + \frac{\mathbf{R}_s^{\mathrm{H}}}{\mathrm{i}\,\omega - \overline{\lambda}_s} \right) \tag{2}$$

Prepared using stcauth.cls
DOI: 10.1002/stc

where $\mathbf{R}_k$ and $\mathbf{R}_s$ are the residue matrices, λ_k and λ_s are the poles, while apex H denotes Hermitian. As a major assumption of classical FDD, PSD matrix $\mathbf{G}_{xx}(\omega)$ is taken constant for stationary white noise input, by allowing for the development of the traditional FDD framework [8].

Differently from white noise input, the PSD of a seismic signal changes with time and frequency, due to the non-stationary nature of the signal [19]. Despite that, in a specific frequency region $\omega_{Sub} = \mathrm{Sub}(\omega) \in \omega$ some seismic signals may be considered as "*weakly stationary*" [49], i.e. the first two statistical moments (mean and autocorrelation) of the signals do not significantly vary in time. In [44], the reliability of this assumption was demonstrated for an applicative seismic case. Accordingly, over this frequency range, the PSD can be approximately represented as to be merely frequency-dependent, allowing to follow classical PSD computations [49].

Further, for some selected non-white noise input, as for several earthquakes, over the frequency interval ω_{Sub}, which is chosen to include the structural modal frequencies under target (or at least some of them), the spectrum may change rather slowly. The selected frequency interval ω_{Sub} may be defined according to the specific study being undertaken. If the target would be that of predicting the seismic response by modal properties, as it is performed here, the focus would be placed on the lower-frequency global response parameters; if the intent would be that of identifying potential structural damage, a focus on the higher-frequency local response parameters would be considered.

The previous "weakly-stationary" assumption may be better appreciated by looking at Fig. 1, where the El Centro earthquake (later adopted in Section 3) has been taken as an example. Over the specified range between $0\,\mathrm{Hz}$ and $10\,\mathrm{Hz}$, a linear interpolation of the spectrum has been represented. The slightness of its angular coefficient and the flat distribution of the regression residuals suggests that the spectrum may be approximated with reasonable accuracy as to be "weakly stationary" (at least similar to a pink noise, i.e. a signal that falls off at $3\,\mathrm{dB}$ per frequency octave in terms of power at a constant bandwidth [49]). The Gabor Wavelet Transform (GWT) [6] of the adopted earthquake record, despite its global non-stationarity, confirms the assumption of a weakly stationary signal for narrow frequency intervals, too.

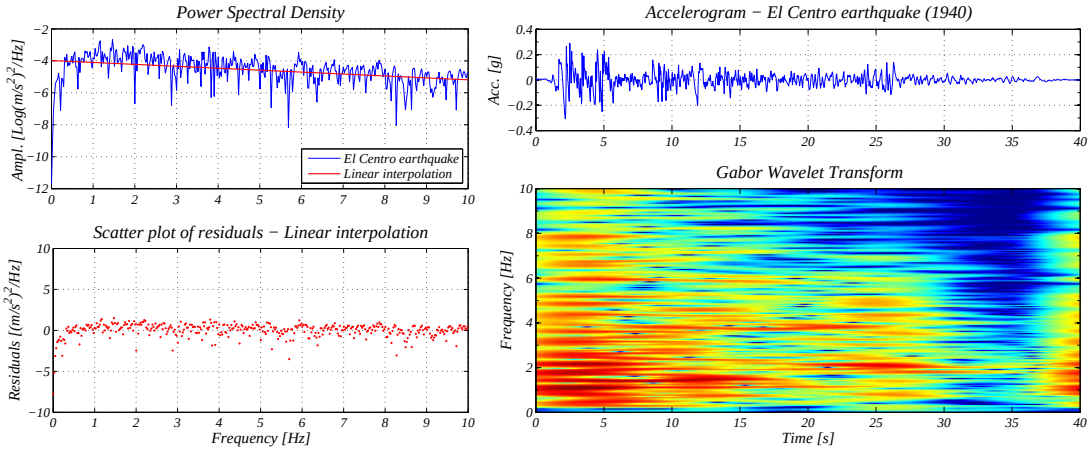

Figure 1. Accelerogram, Auto-PSD with linear regression, residuals and Gabor Wavelet Transform (GWT) of El Centro earthquake (1940).

Thus, by taking into account the previous statements, the spectrum may be considered as about flat, with reasonable accuracy within a frequency range of interest. Therefore, for some selected earthquakes, the frequency dependence of the input PSD matrix for a specific frequency interval may be neglected. Then, for a subset $\omega_{Sub} = \mathrm{Sub}(\omega) \in \omega$, the approximation $\mathbf{G}_{xx}(\omega = \omega_{Sub}) \simeq \mathrm{G}_{xx} = \overline{\mathrm{G}}_{xx}$ keeps reasonably valid.

The present novel analysis of the time-frequency distribution and spectrum flatness is a necessary step when dealing with real earthquake-induced structural response signals, in order to be confident of the correct frequency interval (if a such kind of frequency interval exists) for a reasonable validity of the flat spectrum assumption. For the present work, this time-frequency analysis innovatively

integrates the rFDD algorithm as a mandatory pre-processing step. Basically, a frequency interval must necessarily be found where the spectrum is approximately flat, which contains as much natural frequencies as possible, pertaining to the monitored structure. This procedure, which shall be extended also to the output spectrum, enables for the selection of the correct frequency range, to be adopted in the following computational steps. In fact, when dealing with real seismic signals, it is necessary to select a consistent frequency range, in order to get effective estimates from the application of the rFDD algorithm. Otherwise, it is not possible to ensure the reliability of the achieved estimates. After the selection of the ω_{Sub} interval, the remaining part of the frequency spectrum shall be discarded through an appropriate (low-, band- or high-pass) filtering.

Accordingly, the rFDD theory (and the consequent adoption of real seismic response signals) is valid within the ω_{Sub} frequency interval. Basically, the classical FDD theory [8] is approximately valid within to the ω_{Sub} range of interest. By using the local flatness assumption on the input PSD matrix and by applying the Heaviside partial fraction expansion theorem to Eq. (2), it is possible to obtain the rFDD modal decomposition of the output PSD matrix. This is defined for the frequency interval ω_{Sub}, in the narrow band of spectrum lines in the vicinity of a modal frequency:

$$\mathbf{G}_{yy}(\omega_{Sub}) \simeq \sum_{k=1}^{n} \left(\frac{\mathrm{d}_k \overline{\boldsymbol{\phi}}_k \boldsymbol{\phi}_k^{\mathrm{T}}}{\mathrm{i}\,\omega - \lambda_k} + \frac{\mathrm{d}_k \overline{\boldsymbol{\phi}}_k \boldsymbol{\phi}_k^{\mathrm{T}}}{-\mathrm{i}\,\omega - \overline{\lambda}_k} \right) \Bigg|_{\omega=\omega_{Sub}} = \overline{\boldsymbol{\Phi}} \left\{ \mathrm{diag} \left[\Re\mathrm{e} \left(\frac{2\mathrm{d}_k}{\mathrm{i}\,\omega - \lambda_k} \right) \right] \right\} \boldsymbol{\Phi}^{\mathrm{T}} \tag{3}$$

where $\mathrm{d}_k \overline{\boldsymbol{\phi}}_k \boldsymbol{\phi}_k^{\mathrm{T}}$ is the Hermitian residue matrix of the PSD output corresponding to the k$^{\mathrm{th}}$ pole λ_k, being $\boldsymbol{\phi}_k$ the k$^{\mathrm{th}}$ modal vector. Then, due to the assumption on $\mathbf{G}_{xx}(\omega)$, d_k turns out to be a real scalar. The approximation of Eq. (3) shall be valid also for heavy damping (modal damping ratios ζ_k up to 10% and more), as demonstrated in [43].

The transpose of the PSD matrix $\mathbf{G}_{yy}(\omega_{Sub})$ is then decomposed, at discrete frequency lines $\omega = \omega_i \in \omega_{Sub}$, by using a Singular Value Decomposition (SVD) [5], by achieving an expression that is effective also for close modes [5, 26]. When only the q$^{\mathrm{th}}$ principal value is dominant (i.e. it reaches a maximum near the modal frequency ω_q), the response PSD matrix can be approximated by a unitary rank matrix [8], as stated by classical FDD methods [5]:

$$\mathbf{G}_{yy}^{\mathrm{T}}(\omega_i = \omega_q) \simeq \mathbf{s}_q \mathbf{u}_{q1} \mathbf{u}_{q1}^{\mathrm{H}} \tag{4}$$

where the first SV $\mathbf{s}_q$ at the q$^{\mathrm{th}}$ resonance frequency is an estimate, with unitary normalization, of the related mode shape $\hat{\boldsymbol{\phi}}_q = \mathbf{u}_{q1}$. Finally, in standard FDD analysis the identified mode shape can be compared to the others in its proximity [8], by using the well-known Modal Assurance Criterion (MAC) index [51]. The validity of the estimated mode shapes may be assessed also with further indexes, see e.g. those in [26], or the ones originally adopted in [42], as the Modal Phase Collinearity (MPC) and the Auto-MAC.

2.2. Integrated approach for PSD matrix computation

The output PSD matrix $\mathbf{G}_{yy}(\omega_{Sub})$, selected for the frequency interval ω_{Sub}, shall be computed through numerical methods. The integrated approach for PSD matrix computation presented in this work simultaneously implements the Wiener-Khinchin [5] and the Welch's modified periodogram [62] methods in a consecutive way.

The Wiener-Khinchin algorithm is based on the direct Fourier Transform (FT) of the correlation matrix $\mathbf{R}_{yy}^{\mathrm{detr}}(\tau)$, in order to obtain the PSD matrix of the responses $\mathbf{G}_{yy}^{\mathrm{detr}}(\omega_{Sub})$:

$$\mathbf{G}_{yy}^{\mathrm{detr}}(\omega_{Sub}) = \mathscr{F}\left[\mathbf{R}_{yy}^{\mathrm{detr}}(\tau)\right] = \mathscr{F}\left[\overline{\boldsymbol{\Phi}}\, \mathbf{R}_{pp}^{\mathrm{detr}}(\tau) \boldsymbol{\Phi}^{\mathrm{T}}\right] = \overline{\boldsymbol{\Phi}}\, \mathbf{G}_{pp}^{\mathrm{detr}}(\omega_{Sub}) \boldsymbol{\Phi}^{\mathrm{T}} \tag{5}$$

where $\mathbf{G}_{pp}^{\mathrm{detr}}(\omega_{Sub}) = \mathscr{F}\left[\mathbf{R}_{pp}^{\mathrm{detr}}(\tau)\right]$ is the response PSD matrix (in terms principal coordinates p_i), obtained as FT of the untrended correlation matrix $\mathbf{R}_{pp}^{\mathrm{detr}}(\tau)$ (see [44] for more details), expressed again in principal coordinates. Then, this method shall be called *Correlation Approach (Corr)*.

DOI: 10.1002/stc

After the use of the Corr approach, the second method adopted by rFDD for the estimation of the $\mathbf{G}_{yy}(\omega_{Sub})$ matrix derives from the Welch modified periodogram, starting from [62]:

$$\mathbf{G}_{yy}(\omega_{Sub}) \simeq \frac{1-r}{K} \sum_{k=1}^{K/(1-r)} \frac{\left[\sum_{t=0}^{L-1} \overline{\mathbf{y}}_k(t)\mathrm{W}(t)e^{-\mathrm{i}\omega\frac{t}{L}}\right]\left[\sum_{t=0}^{L-1} \mathbf{y}_k^{\mathrm{T}}(t)\mathrm{W}(t)e^{-\mathrm{i}\omega\frac{t}{L}}\right]}{\left[\sum_{t=0}^{L-1} \mathrm{W}(t)^2\right]} \tag{6}$$

where K is the number of segments of length L and overlapping r ($r = 2/3$ in the present work) in which the initial signal $\mathbf{y}(t)$ has been divided, $\mathbf{y}_k(t)$ is the k$^{\text{th}}$ segment of the original signal and $\mathrm{W}(t)$ is the considered windowing function, i.e. an Hanning window as in this case [5]. The method resumed in Eq. (6) shall be called *Welch Approach (Welch)*.

The present rFDD algorithm displays the innovative and powerful feature of the simultaneous implementation of both Corr and Welch methods, into an integrated process. First, a run with the Corr approach is performed, by applying the peak-picking procedure on the sharper and better defined SVs provided by this method. The peak-picking technique is supported by the use of MAC, Auto-MAC, MPC and Auto-MPC indexes, through comparison of the mode shapes of each potential peak with those of the others in its proximity. In this way the correct peaks (i.e. the correct frequency lines related to the modes of vibration) may be detected. This method works well especially with short signals, though it may produce slightly less accurate mode shapes. Peaks may be detected not only on the first SV curve, but also on the remaining ones.

Then, the PSD matrix is recomputed through the Welch's approach, which is applied sequentially to the Corr method. This aims at extracting the final modal estimates, read in correspondence to the formerly-detected frequency lines. This method implements averaging and windowing, before frequency-domain convolution, leading to slightly better estimates, especially with long recordings, despite the appearance of noisier singular values. With this method, only the peaks on the first SV are adopted, in order to avoid leakage on the achievable estimates.

As opposed to previous rFDD attempts in [43, 44] with pseudo-experimental (synthetic) seismic response signals, this original integrated procedure leads to a substantial improvement of the seismic modal estimates in case of real earthquake input, as analysed here. In fact, for real seismic response signals, this procedure is automatically and systematically performed by the rFDD algorithm. Otherwise, identification may become difficult, often unreliable or actually mistaken. This potential feature can be appreciated in Fig. 2, where the two methods for the computation of the PSD matrix are sequentially displayed, focusing on the results (i.e. on the detected frequency lines) provided by the subsequent SVD computation.

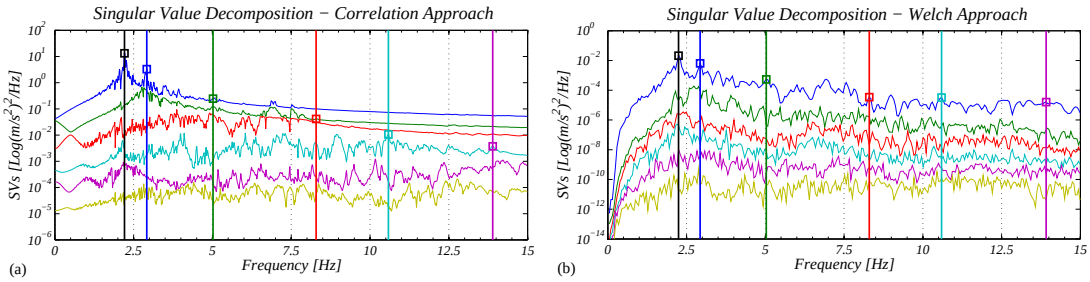

Figure 2. Singular Value Decomposition obtained from integrated computation of the PSD matrix: (a) Corr Approach; (b) Welch Approach; response to Encino earthquake (2014), NS component. The peaks frequency lines detectable in the Corr Approach (a) are transferred to the Welch Approach (b), where the modal peaks are hardly visible for direct peak-picking.

2.3. Strong-motion modal parameter estimates via the rFDD approach

Conceptually, the rFDD approach derives from traditional FDD methods [8], which shall not be adequate in principle to deal with earthquake-induced response signals. The rFDD algorithm

DOI: 10.1002/stc

has been specifically developed for strong ground motion modal parameter estimates, also at simultaneous heavy damping (in terms of identification challenge). The novel procedures proposed in Sections 2.1 and 2.2 enhance the rFDD method, when dealing with real earthquake-induced responses (see Steps 1, 2, 4). The remaining steps (Steps 3, 5-8) rely on previous work [43, 44], and are reported here for the sake of completeness. The work-flow of the present implementation for real seismic response signals may be summarized by the following computational steps:

1. Pre-processing time-frequency analysis (Section 2.1), aiming at a correct evaluation of the signal characteristics (non-stationary features, validity of the weakly-stationary and spectrum flatness assumptions) and of the frequency range which shall be selected for the analysis.
2. Specific data filtering applied to the input (response) signals before starting the identification procedure; type, cut-off and/or bandpass frequencies and orders shall be selected as a function of the outcomes (boundaries of the frequency interval) of the time-frequency spectrum analysis (Section 2.1).
3. Processing of the auto- and cross-correlation matrix, which may be further manipulated to obtain an untrended well-defined version, $\mathbf{R}_{yy}^{\mathrm{detr}}(\tau)$; this helps in removing possible troubles related to weakly-stationary or non-stationary data, by achieving clearer and well-defined SVs, with a sort of "SVs filtering" [44].
4. Integrated PSD matrix computation, implementing sequentially both Wiener-Khinchin [5] and Welch's modified periodogram [62] methods (Section 2.2).
5. Estimation of modal parameters by operating on different SVs and on their composition, without the need of Blind Source Separation methods [13].
6. Inner procedure for frequency resolution enhancement, without the need of higher frequency sampling [43].
7. Combined use of different MAC indexes (MAC, Auto-MAC, MPC, Auto-MPC) towards modal validation purposes, as preliminary traced in [44].
8. Identification of modal damping ratios by an iterative optimization algorithm, as detailed in [43, 44], where the enhancement of the damping ratio estimates with respect to classical EFDD was demonstrated by using synthetic earthquake response data only. Here, the iterative procedure is applied to real seismic response data, and is proven to be effective in identifying reliable modal damping ratios, especially when dealing with heavy structural damping in terms of identification challenge.

One may notice that, despite certainly requiring an expert user, the application of this research rFDD algorithm (not a commercial software) is *not subjective* at all and that, by following the systematic steps above, consistent modal dynamic identification by adopting real earthquake-induced response signals can be achieved through the present implementation, as it is going to be demonstrated by the outcomes reported in the following sections.

3. PRIOR NUMERICAL VALIDATION OF THE ENHANCED rFDD METHOD

Beyond first numerical attempts with shear-type frames and synthetic response signals that were performed in [42–44], here two additional numerical trials are prior proposed for the validation of the enhanced rFDD algorithm in view of its subsequent use with real seismic response signals. First, a fixed-base 5-storey frame is considered in Section 3.1, by assuming two types of structural damping. Then, a 5-storey frame with Soil-Structure Interaction (SSI) effects is modelled and adopted for the analyses in Section 3.2. The achieved results may be compared to known target values and estimates coming from [19], where an output-only identification procedure conceived to work with strong ground motion responses was developed. As it will be presented by the following analyses, current results look to be superior and basically confirm the efficacy of the developed algorithm in the present framework.

DOI: 10.1002/stc

3.1. Simulated 5-storey structure

The structure under analysis for the first part of the present numerical validation is a fixed-base 5-storey shear-type frame, taken from [19]. Table I summarizes stiffness and mass properties for all the floors. As it concerns damping, two different cases are considered:

- Stiffness proportional damping (ζ_s); first mode modal damping ratio is set to 0.5%.
- Mass proportional damping (ζ_m); first mode modal damping ratio is set to 10%.

The input motion is taken as the 1940 El Centro earthquake (18/05/1940, Station 0117, NS component) [11], which is adopted as base-excitation for the structure. It is characterized by $\mathrm{M} = 7.1$, duration $t = 40\,\mathrm{s}$, sampling frequency $f_s = 100\,\mathrm{Hz}$ and $\mathrm{PGA} = 0.312\,\mathrm{g}$. The structural response is calculated via Newmark's direct integration method (average acceleration) [12].

Table I. Properties of the 5-storey frame [19].

Floor	1	2	3	4	5
Stiffness $\times 10^3$ [kN/m]	350	280	210	140	70
Mass $\times 10^3$ [kg]	300	300	300	300	300

Figure 3 represents the Auto-PSD and GWT related to the first floor and to the roof of the 5-storey frame, using both stiffness and mass proportional damping. The ridges detection on the GWTs confirm the local weakly stationary of the response signals, which allows for the handling by the present rFDD procedure. All the modes are identifiable in the graphs, starting from the first floor motions, due to the excitation features and to the fixed-base conditions. This can be seen also through the PSD peaks. As expected, first modes of vibration display higher energy in the stiffness proportional system, while this is true for the last modes of the mass proportional system. This is directly related to the modal damping ratio associated to each resonance frequency. Then, because of light damping associated to the higher modes, the system with mass proportional damping shows better modal parameter estimates, despite the heavy damping associated to the first modes, as it can be seen by the results reported in Table II. The estimates are very accurate for both cases, by showing MAC values that turn out always higher than 0.95, and identified natural frequencies and modal damping ratios very close to the target values.

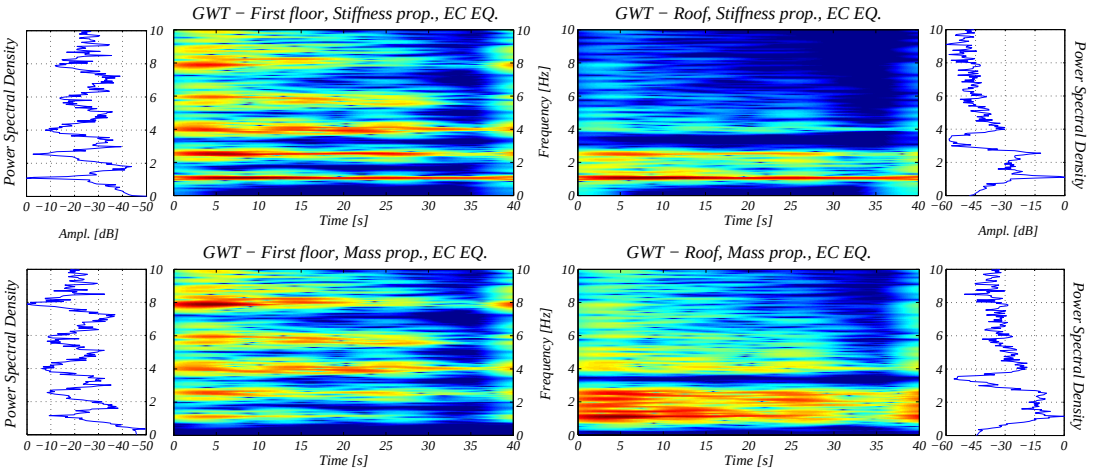

Figure 3. Auto-PSD and Gabor Wavelet Transform (GWT) of the 5-storey frame, first floor (left) and roof (right) channels, stiffness (top) and mass (bottom) proportional dampings, El Centro earthquake.

DOI: 10.1002/stc

Table II. Comparison between target and identified (ID) modal dynamic properties, stiffness and mass proportional dampings, El Centro earthquake, 5-storey frame.

Mode	*Target*			*ID, Stiffness prop. damp.*			*ID, Mass prop. damp.*		
	f_n [Hz]	ζ_s [%]	ζ_m [%]	f_n [Hz]	ζ_s [%]	MAC	f_n [Hz]	ζ_m [%]	MAC
1	1.112	0.50	10.0	1.114	0.51	1.000	1.111	9.87	1.000
2	2.560	1.15	4.34	2.564	1.08	1.000	2.567	4.26	0.997
3	4.047	1.82	2.75	4.016	1.84	0.999	4.016	2.74	0.999
4	5.665	2.55	1.96	5.591	2.50	0.989	5.658	1.87	0.996
5	8.135	3.66	1.37	7.935	3.58	0.952	8.011	1.46	0.993

3.2. Simulated Soil-Structure Interaction system

For the second part of the numerical validation, the previous 5-storey fixed-base shear-type frame has been set on a flexible foundation. Soil-Structure Interaction (SSI) effects have been simulated via a Sway-Rocking model, which has added two degrees of freedom to the system, i.e. the foundation sway and the system rocking (more details on this model may be found in [45,46,52] and references quoted therein).

Floor mass and inter-storey stiffness are kept as before, as well as the shaking earthquake (1940 El Centro earthquake). The inter-storey height is assumed to be $4\,\mathrm{m}$. The mass moment of inertia for each floor is taken as $I_i = 7.5 \times 10^6\,\mathrm{kg\,m^2}$. The adopted foundation displays a mass $m_0 = 5 \times 10^5\,\mathrm{kg}$ and a mass moment of inertia $I_0 = 7.5 \times 10^6\,\mathrm{kg\,m^2}$. Finally, sway and rocking soil stiffnesses are set equal to $k_s = 9 \times 10^8\,\mathrm{N/m}$ and $k_r = 3 \times 10^{10}\,\mathrm{N\,m}$, respectively.

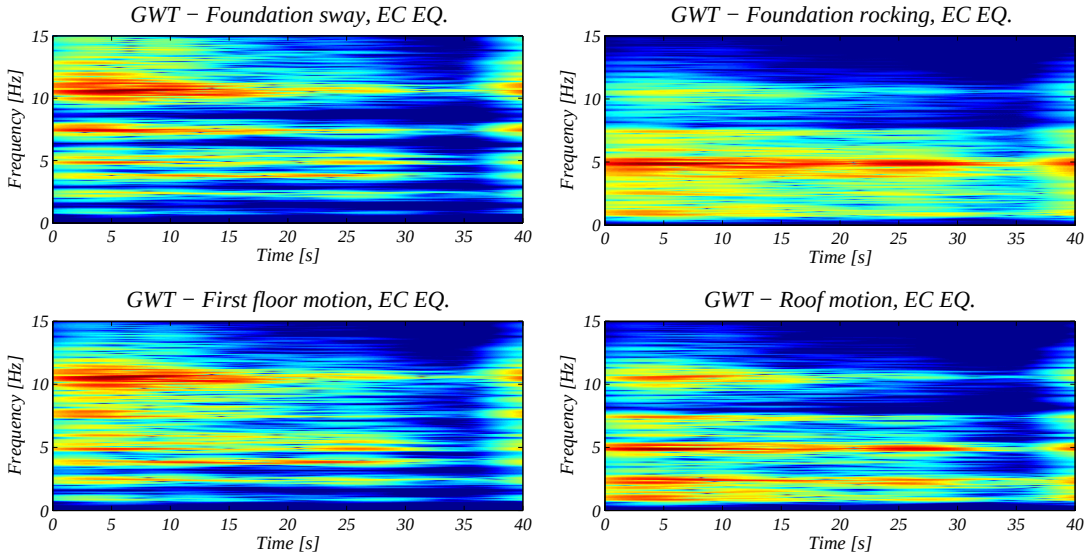

Figure 4. Gabor Wavelet Transform (GWT) of the 5-storey SSI sway-rocking frame, foundation sway, rocking, first floor and roof motions, mass proportional damping, El Centro earthquake.

For the sake of compactness, only mass proportional damping has been considered here, with first modal damping ratio set again to 10%. Figure 4 represents the GWT related to the 5-storey sway-rocking system, for the foundation sway, rocking, first floor and roof motions. It is possible to appreciate that not all the modes may be detected in all the degrees of freedom. This fact is directly related to more difficult modal parameter estimates, with respect to the standard fixed-base 5-storey frame (without SSI effects). Also, the presence of SSI effects is clearly visible, since ridges related to structural frequencies may be detected in the foundation motions, as well as for soil (non-structural) frequencies in the above structural motions.

Prepared using stcauth.cls
DOI: 10.1002/stc

Table III. Comparison between identified and target modal dynamic properties, use of 5 or 7 sensors, mass proportional damping, El Centro earthquake, 5-storey SSI sway-rocking frame.

Mode	*Target*		*ID, 5 sensors*			*ID, 7 sensors*		
	f_n [Hz]	ζ_m [%]	f_n [Hz]	ζ_m [%]	MAC	f_n [Hz]	ζ_m [%]	MAC
1	0.9052	10.0	0.9384	10.7	1.000	0.9392	9.85	1.000
2	2.450	3.70	2.464	3.73	0.999	2.399	3.69	0.997
3	3.873	2.34	3.882	2.37	1.000	3.876	2.34	0.999
4	4.914	1.85	4.894	1.82	1.000	4.901	1.83	0.996
5	5.428	1.67	5.396	1.58	0.949	5.383	1.65	0.993
6	7.565	1.20	7.446	1.24	1.000	7.538	1.22	0.993
7	10.97	0.83	10.88	0.86	0.999	10.96	0.84	0.993

Nevertheless, estimates are still very accurate, whether by using the full 7-channel set of records or by using a reduced 5-channel set (without foundation sway and rocking recordings). All the modes are identified correctly. In fact, MAC values are always higher than 0.94, and natural frequency and modal damping ratio estimates are still very close to the target values. Then, the rFDD algorithm proves its effectiveness in dealing also with earthquake-induced structural recordings affected by SSI effects, by working with full output-only conditions, without the need of knowing the foundation input motions.

4. APPLICATION OF THE rFDD APPROACH TO REAL EARTHQUAKE-INDUCED RESPONSE SIGNALS

4.1. Real monitoring case-study description

After the prior numerical validation reported in Section 3 for synthetic response signals, the present rFDD algorithm is applied to real earthquake-induced response signals recorded on the Van Nuys Hotel, California (Fig. 5). Data are taken from the Center of Engineering Strong Motion Data (CESMD) online database [11]. This building has been selected as a well-documented case, displaying a good spatial layout of instrumentation and considerable wealth of recorded data. Also, pre- and post-retrofitting data before and after the 1994 Northridge earthquake are available.

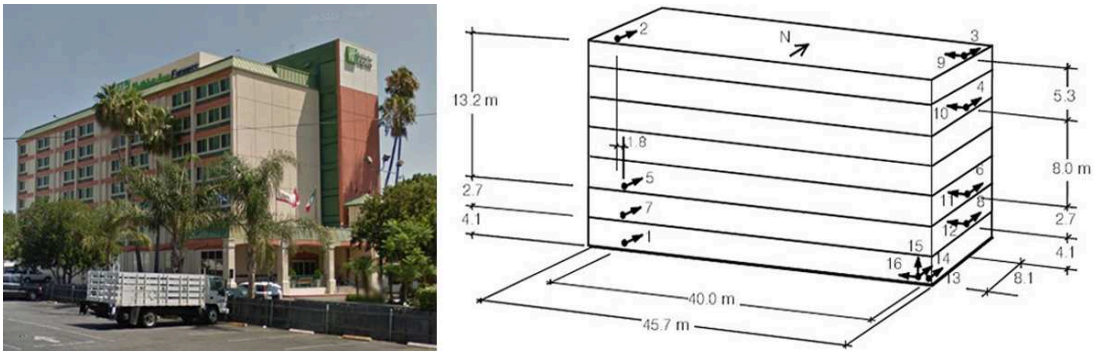

Figure 5. External view of the VN7SH building and three-dimensional sensor layout (adapted from [32]). Input data are taken from the CESMD database.

The 7-storey RC hotel building (in short VN7SH) is located in Van Nuys, central San Fernando valley, metropolitan Los Angeles area, California [29, 32, 57]. It was designed in 1965 and constructed in 1966, according to the existing Building Code [32]. The structure displays a plan of $45.72\,\mathrm{m} \times 18.90\,\mathrm{m}$, for an approximate total floor surface of $6200\,\mathrm{m}^2$. At the time of construction, the framing consisted of columns spaced of $6.10\,\mathrm{m}$ in the transverse direction and of $5.80\,\mathrm{m}$ in the

DOI: 10.1002/stc

longitudinal direction. Spandrel beams surround the perimeter of the structure and, jointly with the exterior columns, form the primary resisting frame to the lateral loads, in each direction. With the exception of some light framing members supporting the stairway and the elevator openings, the structure is essentially symmetric. The floors display RC flat slabs, with the following thicknesses: $25\,\mathrm{cm}$ at the 2^{nd} floor, $22\,\mathrm{cm}$ between the 3^{rd} and the 7^{th} floor and $20\,\mathrm{cm}$ at the roof. The foundation system consists of a group of piles, with a diameter of $60\,\mathrm{cm}$ and a length of $12.20\,\mathrm{m}$. The structure sits on a recent alluvium soil; primarily, it consists of sandy silts and silty fine sands [29, 32].

During its life, the structure has been debilitated by the 1971 San Fernando earthquake (09/02/1971, $\mathrm{M_W} = 6.6$) and severely damaged by the 1994 Northridge earthquake (17/01/1994, $\mathrm{M_L} = 6.4$), event after which the building was considerably retrofitted. Extensive structural damage occurred as column-beam/column joints shear failures along the perimeter of the frame. Failures also included spalling of the covering concrete over the longitudinal bars, buckling of the longitudinal bars and through-cracks up to several centimetres wide. In this regard, noticeable surveys and analyses can be found in [29, 57–59]. Structural repairs and strengthening after the 1994 Northridge earthquake involved the addition of shear walls at three columns of the south frame and four columns of the north frame, and at several interior column lines. Base fixity was provided to the new shear walls by the addition of grade beams spanning between pier groups [32]. Fig. 5a shows a picture resembling the actual conditions of the building.

According to the California Strong Motion Instrumentation Program, the building was instrumented in 1980 (CSMIP Station n. 24386) [11]. The recording system consisted of 16 accelerometers on five levels of the building: five channels were devoted to the EW direction, while ten to the NS and one to the UP direction. Fig. 5b briefly represents the overall building dimensions and the instrumentation layout.

4.2. Strong ground motion data set and properties

In the present work, earthquakes pertaining to both the pre-, during- and post-1994 Northridge earthquake are considered. Specifically, response data belong to two set of earthquakes, i.e. the four earthquakes occurred from 1987 to 1994 (pre-retrofit) and the five earthquakes occurred from 2008 to 2014 (post-retrofit), including the recent 2014 Californian events of Encino and Westwood Village. Their main characteristics and properties are summarized in Table IV.

Recorded data belong to the four EW channels and to the six NS channels (the channels at the ground floor have not been considered, both for the OMA purposes of the present analysis and for the low signal-to-noise ratio). Because of the limited number of sensors along the height of the building (4 monitored floors on a total of 7 storeys), the mode shapes show to be slightly less resolute (see subsequent results in Section 5.1 and 5.2), but anyway relevant in engineering terms. Then, following Section 4.3 presents some crucial considerations on the seismic data processing of the strong ground motion response signals.

Table IV. Main characteristics and properties of the adopted set of earthquakes (CESMD database).

Pre-retrofit earthquakes	*Date*	*Dur.* [s]	f_s [Hz]	*M*	*Dist.* [km]	*PGA* [g]	*PSA* [g]
Whittier (WH)	01/10/1987	40	50	6.1	40.0	0.170	0.200
Landers (LA)	28/06/1992	80	50	7.3	187.8	0.040	0.190
Big Bear (BB)	28/06/1992	40	50	6.5	151.6	0.030	0.060
Northridge (NO)	17/01/1994	60	50	6.4	7.0	0.470	0.590
Post-retrofit earthquakes	*Date*	*Dur.* [s]	f_s [Hz]	*M*	*Dist.* [km]	*PGA* [g]	*PSA* [g]
Chinohills (CH)	29/07/2008	95	100	5.4	71.5	0.054	0.140
Borrego Springs (BS)	07/07/2010	62	200	5.4	203.8	0.004	0.016
Newhall (NH)	01/09/2011	58	200	4.2	15.1	0.006	0.016
Encino (EN)	17/03/2014	60	200	4.4	9.8	0.144	0.219
Westwood Village (WV)	01/06/2014	57	200	4.2	13.9	0.010	0.012

4.3. Remarks on the processing of real earthquake-induced response signals

The algorithm's efficiency with real earthquake response data is influenced by several factors, as the signal's characteristics and processing. A first crucial issue concerns the selection of the correct frequency range which shall be adopted in the computational steps, as detailed in Section 2.1.

Another feature belongs to the sampling frequency (f_s) of the recordings, since it may affect the frequency resolution of the PSD matrix. In fact, a poorly defined frequency sampling produces a limitation of the number of FFT points and of the signal decimation, which directly influence the goodness of the estimates. An adequate frequency resolution may be expected of at least $100\,\mathrm{Hz}$, since lower values may produce difficulties in the estimations. In fact, the most demanding estimates derive from the pre-retrofit earthquakes, which are all characterized by $f_s = 50\,\mathrm{Hz}$ (see Section 5.1).

Another important aspect which may affect the frequency resolution of the PSD matrix is related to the shortness of the earthquake acquisitions (with respect to the wideness of the commonly adopted ambient recordings). Then, with the present earthquake-induced response data the frequency resolution (and then the number of points for the PSD matrix computation) has been enhanced by adding a zero-response time window at the end of the records [43], similarly to the zero-padding adopted in classical signal analysis [5]. This can improve the frequency resolution, with a sort of interpolation of the frequency spectra. In the literature, it is generally said that registration lengths of about 1000-2000 times the first natural period of the structure often result quite appropriate [51].

Then, the length of the adopted time series has been extended by adding a zero-solicitation time window of $300\,\mathrm{s}$ to the BS, NH, EN and WV earthquakes ($f_s = 200\,\mathrm{Hz}$), of $600\,\mathrm{s}$ to the CH ground motion ($f_s = 100\,\mathrm{Hz}$) and of $1000\,\mathrm{s}$ to all pre-retrofit seismic shakings ($f_s = 50\,\mathrm{Hz}$). The previous issues, which are all related to the sampling frequency and duration of the acquisitions, may be addressed as *sampling frequency effect*: the rFDD algorithm shall successfully deal with this concern, by providing accurate results at real seismic input.

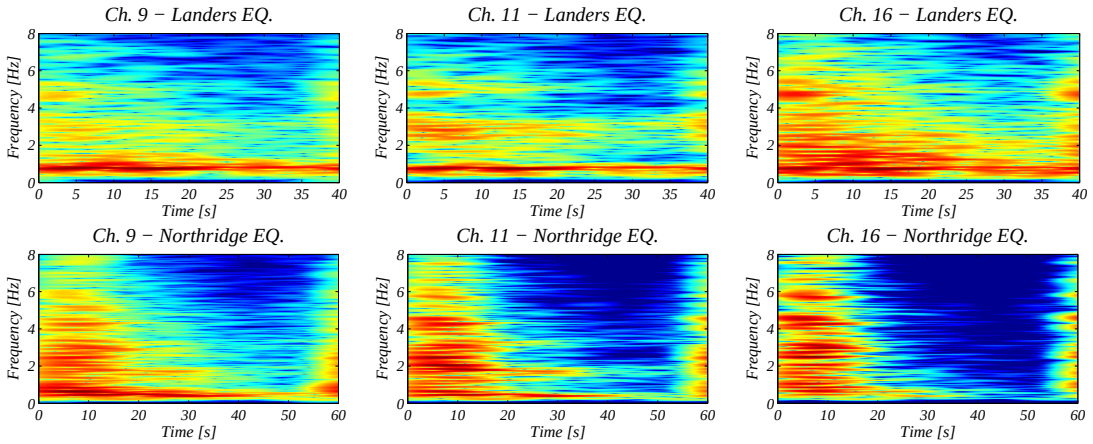

Figure 6. Gabor Wavelet Transform related to Channel 9 (roof), Channel 11 (second floor) and Channel 16 (foundation); response to Landers 1992 (top) and Northridge 1994 (bottom) earthquakes, WE component.

Additionally, another important issue concerns the filtering of data before identification, operation that is strictly related to the frequency interval adopted for the correct working of the rFDD algorithm. Figs. 6 and 7 represent the Gabor Wavelet Transforms (GWT) related to the ground floor (Ch. 16), second floor (Ch. 11) and roof plan (Ch. 9) of the Van Nuys building, WE component, LA-NO and EN-WV earthquakes, respectively. The choice falls on these excitations since they turned out the most demanding for the algorithm. Same considerations may be made for the remaining earthquakes, too.

The frequencies on the y-axes are limited to the structural range of interest, which is different in dealing with pre- or post-retrofit conditions. These intervals have shown to be in agreement with the local weakly stationary required for the application of the rFDD algorithm. Also, several

DOI: 10.1002/stc

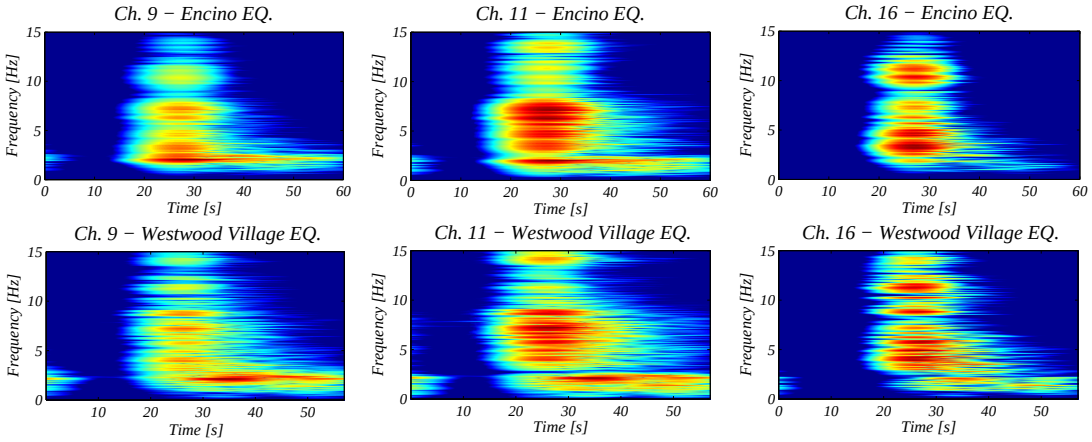

Figure 7. Gabor Wavelet Transform related to Channel 9 (roof), Channel 11 (second floor) and Channel 16 (foundation); response to Encino 2014 (top) and Westwood Village 2014 (bottom) earthquakes, WE component.

attempts with different frequency intervals were made, and basically confirm the reliability of the latter assumption.

Thus, by looking to Figs. 6 and 7, it is possible to see that some structural frequencies can be detected in the ground floor response, as well as the soil frequencies, which may be perceived in the upper structural motions. In particular, pre-retrofit data seem to suffer greater from this issue than post-retrofit data. Some of these frequency ridges are probably related to the harmonics of the seismic event, as well as they may be due to Soil Structure Interaction (SSI) effects, a feature studied by various researchers in relation to the adopted building [32, 58, 59]. A similar effect was seen also in Fig. 4 (Section 3.2), where the numerical 5-storey SSI model has been investigated, confirming the latter hypothesis.

Then, it is clear how the filtering of data before identification looks necessary, with the purpose of setting the frequency range for the rFDD computations, of leaving-out undesired frequency contents and of obtaining less noisy acceleration recordings. In this case, suitably-built low-, band- and high-pass filters have been developed. With appropriate filtering, significant advantages on the achievable rFDD estimates may be obtained.

5. PERFORMED ANALYSES AND MONITORING RESULTS

Several researches in the literature have focused on the identification of the VN7SH modal parameters, based either on ambient tests or on strong motion data recordings, but all are related to signals arising from pre- and during-Northridge (1994) conditions [1, 19, 29, 57–59]. Only Ghahari et al. [19] did output-only (non-FDD) modal identification at seismic input. Therefore, the use of both pre-, during- and post-Northridge acquisitions all together shows to be rather challenging in the present literature, in order to use the present rFDD algorithm with real earthquake-induced response signals (pre-retrofit, Section 5.1) and to estimate the updated modal parameters for the post-retrofit condition (Section 5.2).

5.1. Pre-retrofit conditions

In this subsection the rFDD method is applied to the responses recorded from the pre-retrofit earthquakes. With regards to these pre-repair conditions, several researches have been performed: especially, Trifunac et al. [58, 59] have studied the changes in natural frequencies of the VN7SH building during various earthquakes, using Fourier analysis and Short Time Fourier Transform (STFT) techniques. The identification procedures were based on the analysis of the relative response

DOI: 10.1002/stc

spectra. They concluded that the modal frequencies change among earthquake occurrences and with the intensity of the shaking. They also reported significant Soil Structure Interaction (SSI) effects for this building, which have been thoroughly studied in [32], too.

Ivanovic et al. [29] carried out two detailed ambient vibration tests when the building was damaged by the 1994 Northridge earthquake; they reported estimates of apparent ("pseudo flexible-base") natural frequencies and mode shapes for the damaged building. Alimoradi and Naeim [1] used the 1992 Big Bear and the 1994 Northridge earthquake structural recordings with an EMA technique, i.e. they adopted the ground floor response as input motion. They have extracted pseudo flexible-base modal parameters from these two seismic responses (modal damping ratios, too). Todorovska and Trifunac [57] have performed an impulse response analysis and damage detection of the VN7SH building during several earthquakes, by using wave travel times of vertically-propagating waves. They obtained the first natural frequency of the fixed-base system.

Two approaches have been used by the previous studies to achieve strong ground motion modal parameter estimates, i.e. the adoption of EMA algorithms (by using ground floor responses as input) or the employment of the relative response spectra of the acquired response signals. Both methods appear to be troublesome, since the VN7SH building seems to suffer from SSI effects and the achieving of apparent natural frequencies may not fully describe the soil-structure system.

As a solution of the aforementioned issues, Ghahari et al. [19] suggested to use a specifically-developed OMA technique. They used Time-Frequency distributions and Blind Source Separation methods to extract modal parameter estimates from the VN7SH earthquake response signals. In that work, they have also reported and critically reviewed the previous studies which have been attempted to identify the modal characteristics of the VN7SH building.

Here, the present rFDD algorithm is applied as a plain output-only technique in Frequency Domain to the real earthquake response data recorded on the VN7SH building; strong-motion modal parameters are estimated for all the considered earthquakes, without the need of accounting for the foundation input motion or for the ground floor response.

Among the adopted pre-retrofit seismic excitations, the 1994 Northridge earthquake (NO) severely damaged the VN7SH building [57]. In fact, the GWT related to the NO structural response in Fig. 6 shows a clear sign of natural frequency changes. The ridges representing the first two natural frequencies were significantly discontinuous with respect to the LA case, hence implying that some structural changes occurred in the building. Accordingly, the NO record was divided into four equally-length segments (15 s), while remaining earthquakes were adopted with their full length. All the considered records (and segments) have been processed by the inner procedure for frequency resolution enhancement in order to achieve an adequate number of spectral frequency lines.

Table V. Identified natural frequencies f_i and modal damping ratios ζ_i from the set of pre-retrofit earthquake responses, WE component.

	Mode	*Whittier* (WH)	*Landers* (LA)	*Big Bear* (BB)	*MEAN* (Pre-)	*North. 1* (NO1)	*North. 2* (NO2)	*North. 3* (NO3)	*North. 4* (NO4)	*MEAN* (NO)
f_i [Hz]	1	0.8742	0.8551	0.8063	0.8451	0.6742	0.5094	0.4361	0.4552	0.5192
	2	2.808	3.207	2.527	2.847	2.069	1.767	1.489	1.318	1.661
	3	5.335	5.170	4.848	5.117	4.294	3.320	3.088	3.333	3.509
ζ_i [%]	1	1.82	3.97	4.66	3.48	4.26	14.2	15.6	13.5	11.9
	2	8.10	4.74	8.75	7.20	8.36	1.97	4.69	9.55	6.14
	3	2.77	6.28	5.43	4.83	1.93	7.13	5.94	7.19	5.55

For the present implementation, only the estimates related to the WE component have been reported. Table V shows the first three identified natural frequencies and modal damping ratios from the set of pre-retrofit earthquakes. Mean values have been calculated and reported for the first three ground motions (pre-Northridge, i.e. WH, LA and BB) and for the NO (NO1–NO4) segments,

DOI: 10.1002/stc

respectively. Since the NO event has severely damaged the building, the pre-retrofit earthquakes were divided in these two subsets, aiming at a more detailed discussion on the results.

Then, Fig. 8 shows the mode shapes related to the estimated modes. Only the first three modes of vibration are sought in the present analysis, mainly due to the limited number of sensors along the height of the building. Additionally, the relevant SSI effects, the heavy-damped conditions and the sampling frequency effect (see Section 4.3) adversely affect the estimation of the following modes.

By looking at the achieved modal estimates, the differences among the outcomes from the segments of the NO record are clearly visible. This confirms that potential structural changes, i.e. damage, occurred in the building, as stated by [29, 57–59], too. Only during the last segment, a little recovering seems to have occurred, as indicated by the slight increase of the first and third natural frequencies. This feature, independently confirmed by the present rFDD OMA analysis, was formerly detected and studied in detail in [57, 58], by alternative EMA techniques. This aspect shall further corroborate the objectivity of the present identification approach. Modal damping ratios, which are more or less stable during the previous earthquakes (WH, LA and BB), show significant changes during the NO excitation, by confirming again the appearance of structural damage. Also, the decrease of the first and third natural frequencies of the building during consecutive earthquakes may be another index of damage, although to a lower extent, with respect to those caused by the NO earthquake.

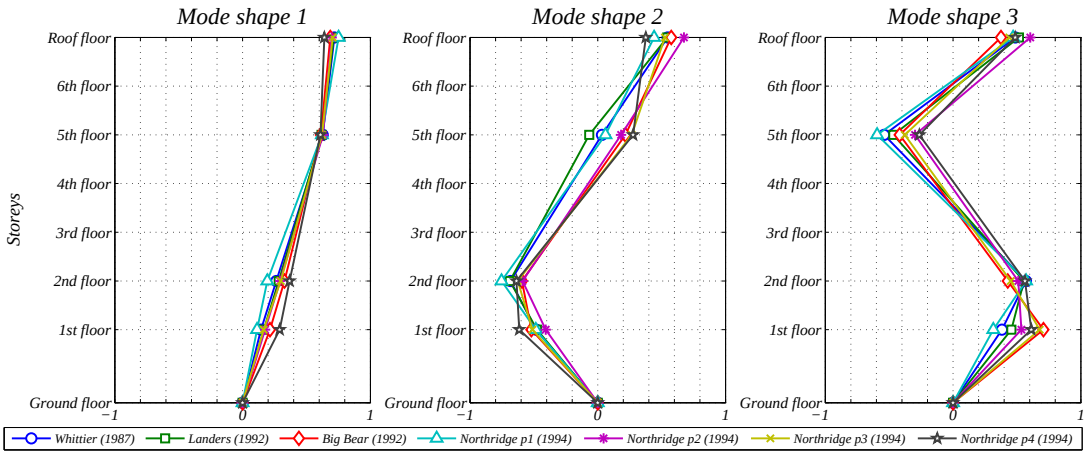

Figure 8. Estimated mode shapes; response to the set of pre-retrofit earthquakes, WE component.

Table VI. Deviations of natural frequencies f_i and modal damping ratios ζ_i with respect to the mean value, pre-retrofit earthquake responses, WE component.

Mean deviation over EQs.	*Whittier* (WH)	*Landers* (LA)	*Big Bear* (BB)	*Nort. 1* (NO1)	*North. 2* (NO2)	*North. 3* (NO3)	*North. 4* (NO4)
f_i [%]	3.04	4.94	7.05	25.65	4.51	12.73	12.67
ζ_i [%]	34.21	26.02	22.59	55.17	38.63	20.71	32.81
Mean deviation over modes	*Pre-retrofit*			*Northridge EQ.*			
	1	2	3	1	2	3	
f_i [%]	3.09	8.43	3.51	14.99	15.48	11.19	
ζ_i [%]	31.74	22.74	28.35	32.09	45.81	32.58	

The previous statements may be confirmed by looking at Fig. 9, where the deviations of frequencies $\Delta f = (f_{est} - f_{targ})/f_{targ}$ and modal damping ratios $\Delta\zeta = (\zeta_{est} - \zeta_{targ})/\zeta_{targ}$ with respect to a target value (taken here as the mean value, for the pre-Northridge earthquakes and NO segments, respectively) are represented in terms of bar-plots, for each earthquake and mode of

vibration. Then, Table VI reports the mean deviations for the considered cases, with respect to the adopted earthquakes (mean of the modes over a specific earthquake) and to the modes (mean of the earthquakes over a specific mode), respectively. The bigger deviations related to the second mode of the pre-Northridge events and the high deviations of all NO segments confirm again the damage scenario which was previously depicted.

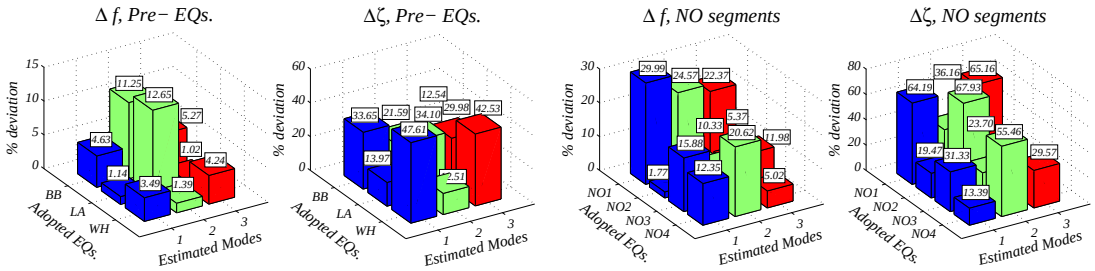

Figure 9. Comparison of frequency and modal damping ratio deviations over the modes of vibration and the set of pre-NO (WH, LA and BB) earthquakes and NO segments.

Then, additional series of indicators are used to assess the validity of the achieved estimates, i.e. the Auto-Modal Assurance Criterion (Auto-MAC) and Auto-Modal Phase Collinearity (Auto-MPC) indexes [44]. The Auto-MAC matrix detects if some modes are not orthogonal to each other, since the diagonal terms are unitary by definition, while off-diagonals ones, due to the orthogonality hypothesis, shall be close to zero. The existence of non-zero off-diagonal terms (e.g. larger than 0.4) can be taken as a sign of little degree of correlation. On the other hand, the Auto-MPC checks the degree of complexity of a mode, by evaluating the functional linear relation between imaginary and real parts of the mode shape components. An MPC index greater than, say, 0.5 may be interpreted as all in-phase mode shape vector components, and the estimates can be considered suitable, while lower values may suggest anomalous fluctuations of the phases (related, for example, to unreliable mode shapes, or to potential structural damage). As for the Auto-MAC, the off-diagonal terms shall be close to zero, otherwise the related modes may not be successfully identified. Both these two indexes help in the estimates and in the validation of the results also when no target parameters are available for comparison purposes, as it is possible to be appreciated in later Section 5.2, where the real post-retrofit cases have been addressed.

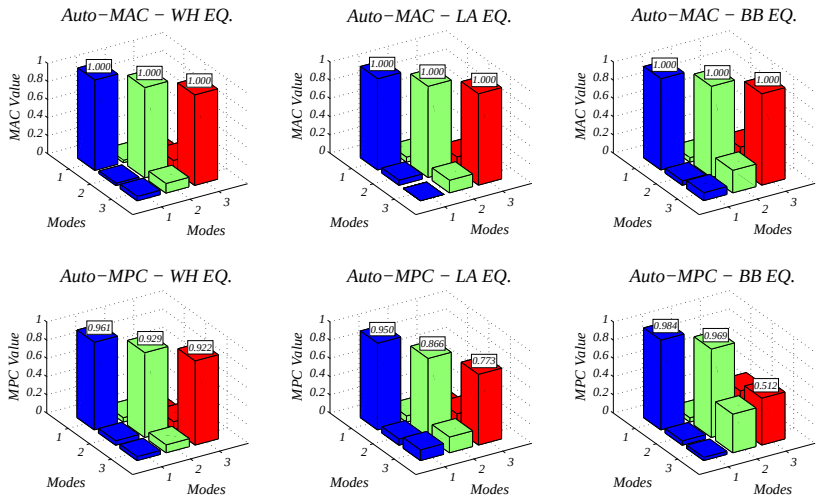

Figure 10. Auto-MAC and Auto-MPC indexes for the estimated mode shapes; pre-NO (WH, LA and BB) earthquakes and NO segments.

DOI: 10.1002/stc

Figs. 10 and 11 represent both indexes as matrix bar-plots for the estimated mode shapes of the pre-NO (WH, LA and BB) earthquakes and NO segments (NO1, NO2, NO3 and NO4), respectively. In particular, with respect to the pre-Northridge earthquakes: there is an increase of off-diagonal terms (Auto-MAC and Auto-MPC) and a decrease of the diagonal terms (Auto-MPC). This is a further index of lower damage during consecutive earthquakes. In relation to the Northridge earthquake: the previous phenomena are considerably higher, and justify the occurred structural damage. Once again, the reliability of the achieved estimates is confirmed.

The presented results can be compared to those from previous literature works, especially those from study [19], compared to which frequencies appears to be very consistent, with average deviations of about 4.14% and 5.97% for the pre-NO and NO segments subsets, respectively. This proves again the efficacy of the rFDD algorithm in detecting modal parameters with real earthquake-induced structural response signals.

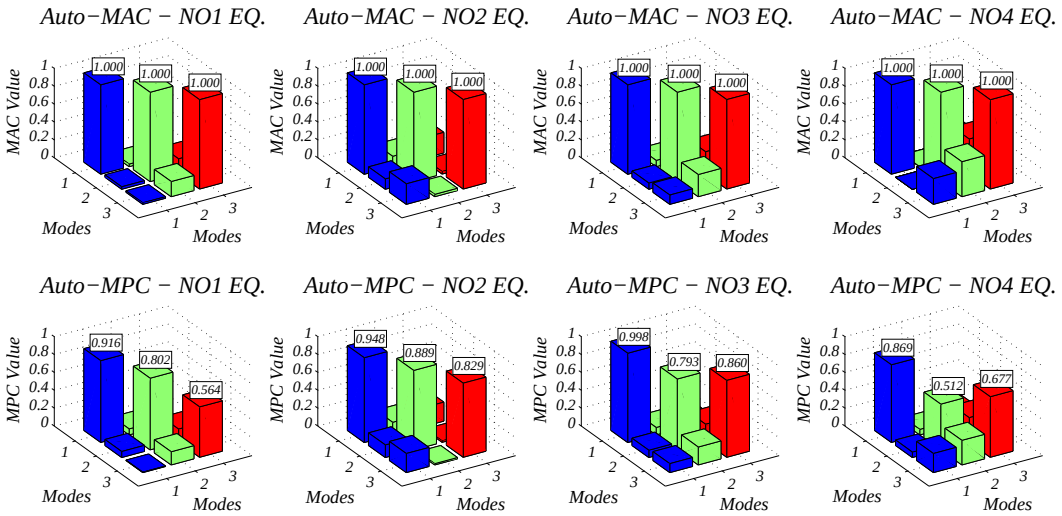

Figure 11. Auto-MAC and Auto-MPC indexes for the estimated mode shapes; NO segments (NO1, NO2, NO3 and NO4) earthquakes.

5.2. *Post-retrofit conditions*

In the present section, comprehensive results for the analysed VN7SH building, subjected to the set of post-retrofit earthquakes outlined in Section 4.2, are reported and analysed. For the VN7SH building, the post-retrofitting stage does not seem to have been considered yet in the present literature for modal dynamic identification purposes. Consequently, there are no target parameters to be compared with. For this reason, some indexes have been used and specifically developed to validate these estimates, too.

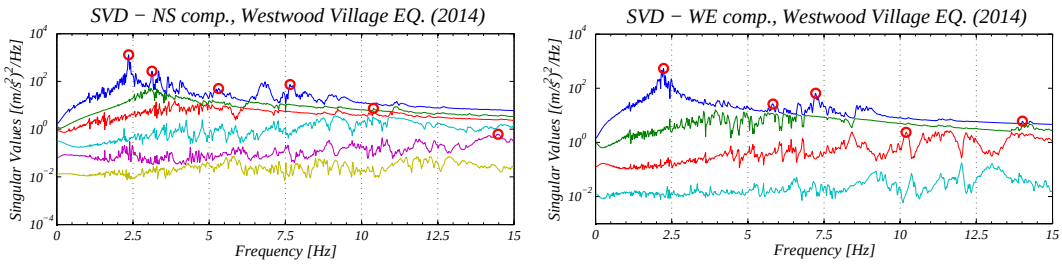

Figure 12. Singular Value Decomposition and peak picking technique by the Corr approach; Westwood Village earthquake, NS (left) and WE (right) components.

DOI: 10.1002/stc

The integrated approach for PSD matrix computation (see Section 2.2) leads to a fundamental support for modal dynamic identification. As a sample, Fig. 12 represents the peak picking on the SVD from the Corr method for the WV earthquake (NS and WE components). Modal peaks are visible on the graphs, and have been identified with circular markers, by operating on different SVs at the same time. Their detection was possible through to the combined use of MAC, Auto-MAC, MPC and Auto-MPC indexes, too. Thus, the integrated approach works well to extract the parameter estimates, by applying then in series the Welch procedure, where the correct peaks may be detected on its noisy SVs, only by relying on the previous outcomes from the Corr approach.

The achieved estimates can be appreciated in Tables VII and VIII, where the identified natural frequencies f_i and modal damping ratios ζ_i are reported, both for the NS and WE components. There is a very good convergence of the estimates over the set of adopted earthquake signals. Only the BS case presents slightly different results, especially in relation to the first mode frequencies. This probably depends on the specific characteristics of this ground motion, which displays the wider epicentral distance and the lower peak ground acceleration (Table IV). This probably leads to a different propagation of the seismic waves and interaction with the structure, and then to slightly different modal estimates.

Table VII. Identified natural frequencies f_i and modal damping ratios ζ_i from the set of post-retrofit earthquake responses, NS component.

	Mode	*Chinohills* (CH)	*Borrego S.* (BS)	*Newhall* (NH)	*Encino* (EN)	*Westwood* (WV)	*MEAN*
f_i [Hz]	1	2.380	2.515	2.324	2.217	2.354	2.358
	2	3.137	3.301	3.184	2.910	3.125	3.131
	3	5.249	4.990	5.039	5.010	5.303	5.118
	4	8.276	8.562	7.900	8.291	7.656	8.137
	5	10.17	10.57	10.48	10.57	10.40	10.44
	6	14.65	13.76	14.77	13.86	14.54	14.31
ζ_i [%]	1	4.41	3.67	4.59	2.64	2.12	3.48
	2	2.20	3.39	3.48	2.48	2.59	2.62
	3	2.54	1.80	3.31	2.08	3.19	2.58
	4	2.90	3.99	4.03	3.85	3.36	3.62
	5	4.14	3.14	3.64	4.88	4.91	4.14
	6	-	-	2.79	-	3.95	-

Table VIII. Identified natural frequencies f_i and modal damping ratios ζ_i from the set of post-retrofit earthquake responses, WE component.

	Mode	*Chinohills* (CH)	*Borrego S.* (BS)	*Newhall* (NH)	*Encino* (EN)	*Westwood* (WV)	*MEAN*
f_i [Hz]	1	2.087	2.246	2.285	2.090	2.227	2.187
	2	5.298	5.781	5.576	5.674	5.811	5.628
	3	7.299	7.168	6.826	7.139	7.217	7.130
	4	10.52	9.785	10.55	10.43	10.27	10.31
	5	13.96	13.76	14.32	13.45	14.01	13.90
ζ_i [%]	1	2.86	2.74	2.61	2.54	2.22	2.59
	2	2.60	4.63	2.96	2.53	3.34	3.21
	3	3.24	2.58	2.93	2.64	2.34	2.75
	4	4.04	3.93	3.72	4.72	5.01	4.28
	5	4.65	4.01	4.91	4.86	4.95	4.68

DOI: 10.1002/stc

Also, the last column of Tables VII-VIII reports the mean of the estimates related to each mode. By looking at these results and at their deviation from the mean, the consistency of the estimates can be appreciated. Deviations of frequencies and modal damping ratios with respect to the mean value might be represented also in terms of bar-plots, for each earthquake and mode of vibration, as done in previous Section 5.1 (see Fig. 9). For the sake of compactness, this is not displayed here. For the frequencies, the maximum deviation is around 7% for the NS component (first mode for the EN case), and just below 6% for the WE component (second mode for the CH case). Instead, for the modal damping ratios, the maximum deviation is 39% for the NS component (first mode for the WV case) and 44% for the WE component (second mode for the BS case).

However, these are only isolated cases: in fact, as it can be deduced from Table IX, the mean deviations for these parameters are lower, settling on average deviations that are less than 3% and 15% for natural frequencies and damping ratios, respectively. Deviations are reported for all the post-retrofit cases, with respect to the adopted earthquakes (mean of the modes over a specific earthquake) and to the modes (mean of the earthquakes over a specific mode), respectively, as done in previous Section 5.1 (see Table VI).

Table IX. Deviations of natural frequencies f_i and modal damping ratios ζ_i with respect to the mean value, post-retrofit earthquakes, NS and WE components.

Mean deviation over EQs.		*Chinohills* (CH)	*Borrego S.* (BS)	*Newhall* (NH)	*Encino* (EN)	*Westwood* (WV)
f_i	$NS\,[\%]$	1.72	4.15	1.85	3.58	1.97
	$WE\,[\%]$	3.06	2.42	2.99	1.96	1.49
ζ_i	$NS\,[\%]$	14.14	17.97	21.20	15.95	19.40
	$WE\,[\%]$	10.69	15.66	6.70	8.26	11.15
Mean deviation over modes		1	2	3	4	5
f_i	$NS\,[\%]$	3.04	2.91	2.46	3.53	1.16
	$WE\,[\%]$	3.60	2.71	1.70	2.19	1.71
ζ_i	$NS\,[\%]$	25.35	17.21	20.61	10.93	14.55
	$WE\,[\%]$	6.52	19.23	9.94	10.87	5.91

As done in previous Section 5.1, the Auto-MAC and Auto-MPC indexes are adopted to assess the validity of the achieved estimates, by taking into account the lacking of target parameters for comparison purposes. Both indexes might be represented as matrix bar-plots for the estimated mode shapes of the adopted earthquakes (similarly to what was done in Figs. 10 and 11). Again, Auto-MAC and Auto-MPC show even more the reliability of the achieved estimates. Only the last MPC indexes (related to the last mode) show slightly poor values in some cases, i.e. the relative mode shapes display some complexity character. This probably depends on the noise brought about by the use of the last SVs for the identification.

Additionally, a parallel between the Auto-MAC and the Auto-MPC over the estimated mode shapes and the set of earthquakes may be conducted, with the purpose of self-comparison within the estimates. This may be done by gradually adopting each of the available earthquakes as a reference case, and by proceeding with comparisons with each remaining seismic instance. Obviously, the closest is the value to 1, the better is the related estimate. Then, all results show to be reliable, since they are characterized by values almost always larger than 0.95 (the lower value is 0.882, 4^{th} mode, EN-WV comparison, WE component) and than 0.90 (the lower value is 0.705, 4^{th} mode, EN-WV comparison, NS component) for the Auto-MAC and Auto-MPC indexes, respectively.

In summary, the careful reading of the presented values and estimates in Tables VII-VIII and the deviations in Table IX (also in relation to pre-retrofit results, where the target values were known) confirm the efficiency and validity of the present rFDD algorithm in working with real earthquake responses, also when no comparison values are available.

Finally, Figs. 13-14 represent a sample of the estimated mode shapes related to the response to the Westwood Village earthquake, NS and WE components, respectively. It is possible to appreciate that, despite for the limited number of sensors along the height of the building, the modes appear anyway clear and effective in engineering terms.

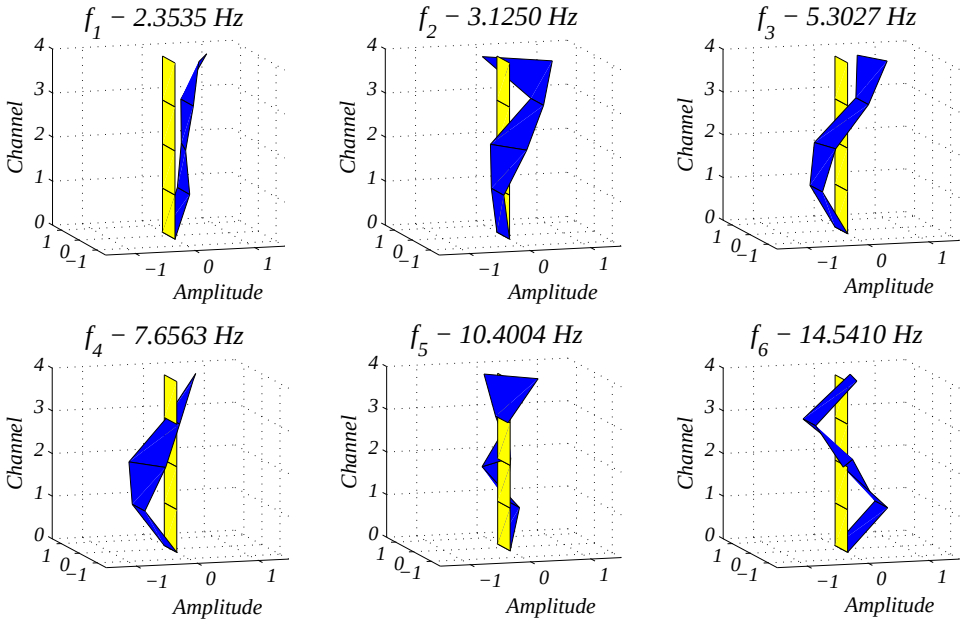

Figure 13. Estimated mode shapes; response to Westwood Village earthquake (2014), NS component.

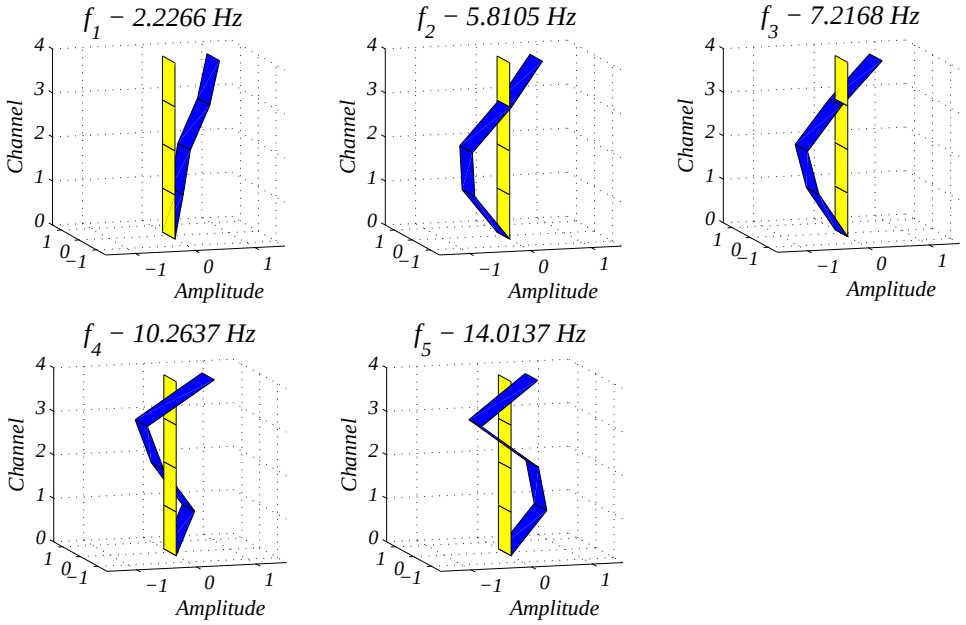

Figure 14. Estimated mode shapes; response to Westwood Village earthquake (2014), WE component.

DOI: 10.1002/stc

5.3. Remarks on the whole identification and monitoring analysis on the VN7SH building

In current Section 5, real earthquake-induced structural response signals taken from the VN7SH building have been adopted towards output-only rFDD modal dynamic identification. Estimates have been extracted for pre-, during and post-Northridge earthquake, namely before ad after the structural retrofit occurred next to the damages of the 1994 Northridge earthquake. Then, the following outcomes and issues may be outlined from the whole analysis attempted on the building:

- The estimate of the VN7SH pre-retrofit modal parameters demonstrates the full effectiveness of the algorithm in dealing with real earthquake-induced response data. Additionally, VN7SH features as close modes, heavy damping, SSI effects and damage have represented a severe trial for the rFDD algorithm, which has anyway returned reliable estimates, as also demonstrated in comparison to achievable literature attempts (Section 5.1).
- The damage scenario recorded for the 1994 Northridge earthquake proves the ability of the present rFDD approach to deal with very short structural recordings and to detect possible damage, i.e. potential structural changes which may affect the structure under seismic Structural Health Monitoring (Section 5.1).
- The estimate of the updated modal parameters of the VN7SH building (post-retrofit stage) by using real earthquake-induced structural response signals looks quite challenging in the present literature, and returns rather reliable estimates, with very good convergence of results. It allows to validate the rFDD algorithm for earthquake Structural Health Monitoring purposes, also when no target or comparison parameters are known (Section 5.2).
- Overall, the estimated mode shapes show a clear and effective representation in engineering terms, both for pre-, during and post-repair conditions, despite for the limited number of sensors adopted along the height of the building. They confirm the overall goodness of the present strong ground motion modal parameter estimates (Sections 5.1-5.2).
- As concerning to the rFDD Structural Health Monitoring outcomes on the analysed VN7SH building, the estimated strong-ground motion modal parameters allow for a rather clear detection of the current modal building properties. In particular, pre-Northridge frequencies and mode shapes indicate a principle of moderate structural damage during subsequent earthquake events. Structural damage becomes explicitly prominent by inspecting the during-Northridge modal parameters. These findings appear in agreement with the available literature studies (Section 5.1). Finally, the post-retrofit monitoring stage clearly shows the actual modal characteristics of the VN7SH building, with appearing stiffening and change in mode shape typologies, by achieving very good convergence of the estimated strong-ground motion modal parameters through the present rFDD implementation, on a ground where the predicting features are unknown and undebated.

6. CONCLUSIONS

The present work has demonstrated the effective development of an enhanced implementation of a *refined Frequency Domain Decomposition (rFDD)* algorithm towards the output-only determination of modal properties from real earthquake-induced response signals, useful for seismic monitoring purposes. First, the enhanced algorithm has been prior validated with simulated data, performed also under Soil-Structure Interaction (SSI) effects, where Soil-Structure modal parameters have been effectively estimated within pure output-only conditions (Section 3.2). Then, real signals taken from the CESMD database on the Van Nuys building have been successfully processed. Consistent estimates of all modal properties have been detected, both for pre-retrofit (Section 5.1) and post-retrofit (Section 5.2) conditions, allowing to illustrate the variation of building properties along the history of the monitored seismic events. This shall prove that the present Frequency-Domain OMA technique may be used for up-to-date detection of building modal properties within Structural Control and Health Monitoring in the Earthquake Engineering range.

As concerning to the main scientific novelties of the present paper, one may consider that, from a theoretical viewpoint, the main implant of the present identification methodology has been already

Prepared using stcauth.cls
DOI: 10.1002/stc

outlined in [43], but for the treatment of *SYNTHETIC* seismic response signals only. On the other hand, the present work addresses specific innovative procedures and improved features, within the same main implant, to allow for the novel processing of *REAL* earthquake-induced response signals. Furthermore, from an application viewpoint, realistic data from an existing building (Van Nuys), available before, during and after the damaging Northridge 1994 earthquake, which has led to building retrofitting, have been successfully analysed through the identification method, by producing a comprehensive analysis, outlining a number of important conclusions related to the context of Structural Health Monitoring for this building, via its identified modal properties.

One may notice that the treated subject of identifying modal properties by employing output-only *SHORT*-duration and *NON-STATIONARY* response time histories with *HEAVY* structural damping, such as the ones encountered in real earthquake response records, appears very challenging in the dedicated literature. Moreover, the present method seems to compete with a rather small number of approaches available on the subject, such as e.g. from [19] itself, devoted to the analysis of the Van Nuys building too, and rather recently from [23, 24], in a different context related to wind engineering. Then, the overall investigation globally sets as a contribution on the stated challenging output-only identification scenario of short-duration, non-stationary, seismic response signals of heavy-damped structures, where current methods are not well developed yet, as instead it shall be for the widely treated case of *LONG*-duration, *STATIONARY*, output-only response time histories of *LIGHTLY*-damped structures.

In the end, main technical outcomes and results on the adoption and application of the present rFDD approach to real earthquake-induced response signals may be summarized below, by outlining the following salient issues:

- The time-frequency signal analysis (Section 2.1), originally implemented here within rFDD, drives the selection of the correct frequency range that shall be adopted in the subsequent computational steps (Section 2.3), as well as for the set-up of the parameters of the procedure. Then, the filtering of data before identification looks an essential step to leave-out undesired frequency contents, which may be very adverse with the processing of real earthquake response signals (Section 4.3).
- The integrated approach for PSD matrix computation (Section 2.2) leads to essential support for modal identification, especially when real earthquake-induced response signals are taken as input channels.
- The estimate of the modal damping ratios takes advantage of the iterative optimization algorithm, by allowing for better modal damping ratio estimates, also with heavy structural damping, in terms of identification challenge (Section 2.3).
- To assess the validity of the estimates, indexes such as the Auto-MAC and Auto-MPC have been specifically developed and adopted, leading to a set of values which allow for modal parameter validation, also when no comparison model data would be available, as in most practical cases (Sections 5.1-5.2).

Further on-going research work may concern attempts with nonlinear structural models, and the use of synthetic earthquake responses and damage scenarios in that context. Also, comparisons with other commonly-used output-only algorithms, additional theoretical and practical investigations on the rFDD approach, adoption and implementation of different Time Domain methods, and identification analysis in the presence of Soil-Structure Interaction effects (within output-only conditions) will be the target of future research investigations.

ACKNOWLEDGEMENTS

The Authors would like to acknowledge public research support from *"Fondi di Ricerca d'Ateneo ex 60%"* and a ministerial doctoral grant and funds at the ISA Doctoral School, University of Bergamo, Department of Engineering and Applied Sciences (Dalmine).

References

1. Alimoradi A, Naeim F (2006), Evolutionary modal identification utilizing coupled shear-flexural response-implication for multistory buildings, Part II: application, *The Structural Design of Tall and Special Buildings*, **15**(1):67–103.
2. Avendano-Valencia LD, Fassois SD (2013), Generalized stochastic constraint TARMA models for in-operation identification of wind turbine non-stationary dynamics, *Proc. of 10th Int. Conf. on Damage Assessment of Structures (DAMAS)*, **1**:587-594, 8-10 July 2013, Dublin, Ireland.
3. Beck J, Jennings P (1980), Structural identification using linear models and earthquake recordings, *Earthquake Engineering and Stuctural Dynamics*, **8**(2):145-160.
4. Beck J (1982), *System identification applied to strong motion records from structures*, Earthquake Ground Motion and its Effects on Structures, Datt S.K. (Ed.), ASME Publications AMD-53: New York; 109-134.
5. Bendat J, Piersol A (1986), *Random Data, Analysis and Measurements Procedures*, Wiley: New York.
6. Boashash B (2003), *Time Frequency Signal Analysis and Processing - A Comprehensive Reference*, Elsevier: Sydney.
7. Brincker R, Ventura C, Andersen P (2001), Damping estimation by Frequency Domain Decomposition, *Proc. of 19th Int. Modal Analysis Conf. (IMAC-19)*, **1**:698-703, 5-8 February 2001, Kissimmee, Florida.
8. Brincker R, Zhang L, Andersen P (2001), Modal identification of output-only systems using Frequency Domain Decomposition, *Smart Materials and Structures*, **10**(3):441-445.
9. Brincker R, Zhang L (2009), Frequency Domain Decomposition revisited, *Proc. of 3rd Int. Operational Modal Analysis Conf. (IOMAC'09)*, **1**:615-626, 4-6 May 2009, Portonovo (Ancona), Italy.
10. Celebi M, Phan LT, Marshall RD (1993), Dynamic characteristics of five tall buildings during strong and low-amplitude motions, *The Structural Design of Tall Buildings*, **2**(1):1-15.
11. CESMD Database (2014), Center for Engineering Strong Motion Data (CESMD), a cooperative database effort from U.S. Geological Survey (USGS), California Geological Survey (CGS) and Advanced National Seismic System (ANSS), available on-line at http://www.strongmotioncenter.org, accessed at 30 September 2014.
12. Chopra AK (2012), *Dynamics of Structures: Theory and Applications to Earthquake Engineering*, 4th Edition, Prentice Hall, Englewood Cliffs: New Jersey.
13. Comon P, Jutten C (2010), *Handbook of Blind Source Separation: Independent Component Analysis and Applications*, Academic Press, Elsevier, Waltham: Massachusetts.
14. Cunha A, Caetano E, Magalhães F, Moutinho C (2013), Recent perspectives in dynamic testing and monitoring of bridges, *Structural Control and Health Monitoring*, **20**(6):853-877.
15. Datta TK (2010), *Seismic Analysis of Structures*, John Wiley & Sons: New York.
16. Diaferio M, Sepe V (2016), Modal identification of damaged frames, *Structural Control and Health Monitoring*, **23**(1):82-102.
17. Doebling S, Farrar C (1999), *The state of the art in structural identification of constructed facilities*, Report by the ASCE Committe on Structural Identification of Constructed Facilities, New York.
18. Garevski M (2013), *Earthquakes and Health Monitoring of Civil Structures*, Springer: New York.
19. Ghahari SF, Abazarsa F, Ghannad MA, Taciroglu E (2013), Response-only modal identification of structures using strong motion data, *Earthquake Engineering and Structural Dynamics*, **42**(11):1221-1242.
20. Ghahari SF, Abazarsa F, Ghannad MA, Celebi M, Taciroglu E (2014), Blind modal identification of structures from spatially sparse seismic response signals, *Structural Control and Health Monitoring*, **21**(5):649-674.
21. Gomez H, Ulusoy H, Feng M (2013), Variation of modal parameters of a highway bridge extracted from six earthquake records, *Earthquake Engineering and Structural Dynamics*, **42**(4):565-579.
22. Gouache T, Morlier J, Michon G, Coulange B (2013), Operational modal analysis with non stationary inputs, *Proc. of 5th Int. Modal Analysis Conf. (IOMAC-2013)*, **1**:1527-1534, 13-15 May 2013, Guimaraes, Portugal.
23. Guo Y, Kareem A (2016), System identification through nonstationary data using Time-Frequency Blind Source Separation, *Journal of Sound and Vibration*, **371**:110-131.
24. Guo Y, Kareem A (2016), Non-stationary frequency domain system identification using time-frequency representations, *Mechanical Systems and Signal Processing*, **72-73**:712-726.
25. Hegde G, Sinha R (2008), Parameter identification of torsionally coupled shear buildings from earthquake response records, *Earthquake Engineering and Structural Dynamics*, **37**(11):1313-1331.
26. Heylen W, Lammens S, Sas P (1998), *Modal Analysis Theory and Testing*, Katholieke Universiteit Leuven, Fac. of Engineering, Dept. of Mechanical Engineering, Div. of Production Engineering, Machine Design and Automation.
27. Hong AL, Betti R, Lin CC (2009), Identification of dynamic models of a building structure using multiple earthquake records, *Structural Control and Health Monitoring*, **16**(2):178-199.
28. Huang C, Lin H (2001), Modal identification of structures from ambient vibration, free vibration, and seismic response data via a subspace approach, *Earthquake Engineering and Structural Dynamics*, **30**(12):1857-1878.
29. Ivanovic SS, Trifunac MD, Novikova EI, Gladkov AA, Todorovska MI (2000), Ambient vibration tests of a seven-story reinforced concrete building in Van Nuys, California, damaged by the 1994 Northridge earthquake, *Soil Dynamics and Earthquake Engineering*, **19**(6):391-411.
30. Karbhari V, Ansari F (2009), *Structural Health Monitoring of Civil Infrastructure Systems*, Woodhead Publishing Limited: Cambridge.
31. Klepka A, Uhl T (2014), Identification of modal parameters of non-stationary systems with the use of wavelet based adaptive filtering, *Mechanical Systems and Signal Processing*, **47**:21-34.
32. Krawinkler H, Ed. (2005), *Van Nuys hotel building testbed report: exercising seismic performance assessment*, Pacific Earthquake Engineering Research Center, Rep. PEER 2005/11, Univ. of California at Berkeley, California.
33. Kun Z, Law S, Zhongdong D (2009), Condition assessment of structures under unknown support excitation, *Earthquake Engineering and Engineering Vibration*, **8**(1):103-114.
34. Lamarche C, Paultre P, Proulx J, Mousseau S (2008), Assessment of the frequency domain decomposition technique by forced-vibration tests of a full-scale structure, *Earthquake Engineering and Structural Dynamics*, **37**(3):487-494.

35. Lei Y, Liu C, Liu LJ (2014), Identification of multistory shear buildings under unknown earthquake excitation using partial output measurements: numerical and experimental studies, *Structural Control and Health Monitoring*, **21**(5):774-783.
36. Lin C, Hong L, Ueng Y, Wu K, Wang C (2005), Parametric identification of asymmetric buildings from earthquake response records, *Smart Materials and Structures*, **14**(4):850-861.
37. Magalhães F, Cunha A, Caetano E, Brincker R (2010), Damping estimation using free decays and ambient vibration tests, *Mechanical Systems and Signal Processing*, **24**(5):1274-1290.
38. Mahmoudabadi M, Ghafory-Ashtiany M, Hosseini M (2007), Identification of modal parameters of non-classically damped linear structures under multi-component earthquake loading, *Earthquake Engineering and Structural Dynamics*, **36**(6):765-782.
39. Michel C, Guéguen P, El Arem S, Mazars J, Panagiotis K (2010), Full-scale dynamic response of an RC building under weak seismic motions using earthquake recordings, ambient vibrations and modelling, *Earthquake Engineering and Structural Dynamics*, **39**(4):419-441.
40. Minami Y, Yoshitomi S, Takewaki I (2013), System identification of super high-rise buildings using limited vibration data during the 2011 Tohoku (Japan) earthquake, *Structural Control and Health Monitoring*, **20**(11):1317-1338.
41. Nagarajaiah S, Yang Y (2016) Modeling and harnessing sparse and low-rank data structure: a new paradigm for structural dynamics, identification, damage detection, and health monitoring, *Structural Control and Health Monitoring*, DOI: 10.1002/stc.1851, available on-line.
42. Pioldi F, Ferrari R, Rizzi E (2014), A refined FDD algorithm for Operational Modal Analysis of buildings under earthquake loading, *Proc. of 26th Int. Conf. on Noise and Vibration Engineering (ISMA2014)*, ISBN: 978-907-3802-91-9, **1**:3353-3368, 15-17 September 2014, Leuven, Belgium.
43. Pioldi F, Ferrari R, Rizzi E (2015), Output-only modal dynamic identification of frames by a refined FDD algorithm at seismic input and high damping, *Mechanical Systems and Signal Processing*, **68-69**:265-291, doi: 10.1016/j.ymssp.2015.07.004.
44. Pioldi F, Ferrari R, Rizzi E (2015), Earthquake structural modal estimates of multi-storey frames by a refined FDD algorithm, *Journal of Vibration and Control*, doi: 10.1177/1077546315608557, available on line.
45. Pioldi F, Salvi J, Rizzi E (2015), FDD modal identification from earthquake response data with evaluation of Soil-Structure Interaction effects, *Proc. of 1st Int. Conf. on Engineering Vibration (ICoEV2015)*, ISBN: 978-961-6536-97-4, **1**:412-421, 7-10 September 2015, Ljubljana, Slovenia.
46. Pioldi F, Salvi J, Rizzi E (2016), Refined FDD modal dynamic identification from earthquake responses with Soil-Structure Interaction, *International Journal of Mechanical Sciences*, doi: 10.1007/s00466-016-1292-0, available on line.
47. Pioldi F, Rizzi E (2016), A Full Dynamic Compound Inverse Method for output-only element-level system identification and input estimation from earthquake response signals, *Computational Mechanics*, **58**(2):307-327, doi: 10.1007/s00466-016-1292-0.
48. Pioldi F, Rizzi E (2016), Full Dynamic Compound Inverse Method: Extension to General and Rayleigh damping, *Computational Mechanics*, in press, doi: 10.1007/s00466-016-1347-2.
49. Priestley MB (1981), *Spectral Analysis and Time Series*, Academic Press: London.
50. Pridham B, Wilson J (2004), Identification of base-excited structures using output-only parameter estimation, *Earthquake Engineering and Structural Dynamics*, **33**(1):133-155.
51. Reynders E (2012), System identification methods for (Operational) Modal Analysis: review and comparison, *Archives of Computational Methods in Engineering*, **19**(1):51-124.
52. Salvi J, Pioldi F, Rizzi E (2015), Effectiveness of seismic-tuned passive Tuned Mass Dampers accounting for Soil-Structure Interaction, *Proc. of 1st Int. Conf. on Engineering Vibration (ICoEV2015)*, ISBN: 978-961-6536-97-4, **1**:641-650, 7-10 September 2015, Ljubljana, Slovenia.
53. Salvi J, Rizzi E (2015), Optimum tuning of Tuned Mass Dampers for frame structures under earthquake excitation, *Structural Control and Health Monitoring*, **22**(4):707-725.
54. Singh JP, Agarwal P, Kumar A, Thakkar SK (2014), Identification of modal parameters of a multistoried RC building using ambient vibration and strong vibration records of Bhuj eartquake, 2001, *Journal of Earthquake Engineering*, **18**(3):444-457.
55. Smyth A, Pei J, Masri S (2003), System identification of the Vincent Thomas Bridge using earthquakes records, *Earthquake Engineering and Structural Dynamics*, **32**(3):339-367.
56. Sun H, Betti R (2014), Simultaneous identification of structural parameters and dynamic input with incomplete output-only measurements, *Structural Control and Health Monitoring*, **21**(6):868-889.
57. Todorovska MI, Trifunac MD (2008), Impulse response analysis of the Van Nuys 7-storey hotel during 11 earthquakes and earthquake damage detection, *Structural Control and Health Monitoring*, **15**(1):90-116.
58. Trifunac MD, Ivanovic SS, Todorovska MI (2001), Apparent periods of a building. I: Fourier analysis, *Journal of Structural Engineering*, **127**(5):517-526.
59. Trifunac MD, Ivanovic SS, Todorovska MI (2001), Apparent periods of a building. II: Time-frequency analysis, *Journal of Structural Engineering*, **127**(5):527-537.
60. Ulusoy H, Feng M, Fanning P (2011), System identification of a building from multiple seismic records, *Earthquake Engineering and Structural Dynamics*, **40**(6):661-674.
61. Ventura CE, Brincker R, Andersen P (2005), Dynamic properties of the Painter Street Overpass at different levels of vibration, *Proc. of 6th Int. Conf. on Structural Dynamics (EURODYN)*, **1**:167-172, 4-7 Sept. 2005, Paris, France.
62. Welch PD (1967), The use of Fast Fourier Transform for the estimation of Power Spectra: a method based on time averaging over short, modified periodograms, *IEEE Transactions on Audio and Electroacoustics*, **15**(2):70-73.
63. Wolf JP (1985), *Dynamic Soil–Structure Interaction*, Prentice-Hall, Englewood Cliffs, New Jersey.
64. Zhang L, Wang T, Tamura Y (2010), A frequency-spatial domain decomposition (FSDD) technique for operational modal analysis, *Mechanical Systems and Signal Processing*, **24**(5):1227-1239.